aerospace

MDPI

Article

Parametric Investigation of Leading-Edge Slats on a Blended-Wing-Body UAV Using the Taguchi Method

Spyridon Antoniou [1,2], Stavros Kapsalis [1,2], Pericles Panagiotou [1,2,*] and Kyros Yakinthos [1,2]

[1] Laboratory of Fluid Mechanics and Turbomachinery, Department of Mechanical Engineering, Aristotle University of Thessaloniki, 54124 Thessaloniki, Greece
[2] UAV Integrated Research Center (UAV-iRC), Center for Interdisciplinary Research and Innovation (CIRI), Aristotle University of Thessaloniki, 57001 Thessaloniki, Greece
* Correspondence: peripan@auth.gr

Abstract: The current study investigated the effect of leading-edge slats on the longitudinal stability at high angles of attack of a Blended-Wing-Body (BWB) Unmanned Air Vehicle (UAV). Using a Design of Experiments (DOE) approach and, specifically, the Taguchi method, four leading-edge slat design parameters were investigated on three different levels. These parameters were the slat semi-span, the rotation of the slat element, the extension forward of the leading edge and the downward drop below the leading edge. An L_9 orthogonal array (OA) was used to investigate the influence of these key design parameters using three performance criteria, namely the angle at which pitch break occurs, the corresponding speed and the distance between the Neutral point of each configuration and the Neutral point of the reference platform. The investigation was conducted by using high-fidelity Computational Fluid Dynamics (CFD) methods for each of the nine configurations defined by the L_9 OA, over a range of angles of attack between −4 and 16 degrees. Based on these results, and using a Signal-to-Noise ratio (SNR) analysis, two combinations were eventually derived, one that optimized pitch break angle and speed and one that optimized longitudinal stability. Finally, the Pareto Analysis of Variance (ANOVA) technique was conducted to define the contribution of each of the six design parameters on the selected performance criteria. More specifically, the semi-span seemed to have the most significant effect on pitch break angle and speed, whereas the rotation of the slat element was the most important parameter with regard to static stability.

Keywords: UAV; Blended-Wing-Body; slats; pitch-break; Taguchi; optimization; ANOVA

Citation: Antoniou, S.; Kapsalis, S.; Panagiotou, P.; Yakinthos, K. Parametric Investigation of Leading-Edge Slats on a Blended-Wing-Body UAV Using the Taguchi Method. *Aerospace* **2023**, *10*, 720. https://doi.org/10.3390/aerospace10080720

Academic Editor: Haixin Chen

Received: 21 July 2023
Revised: 9 August 2023
Accepted: 15 August 2023
Published: 17 August 2023

1. Introduction

The Blended-Wing-Body (BWB) was introduced by Liebeck [1] as a novel and efficient configuration for high-speed subsonic commercial aircraft. Following this initial suggestion, several researchers investigated this configuration both for commercial airliner applications [2–4], as well as for cargo transport [5] and Unmanned Air Vehicle (UAV) applications [6–8]. Especially concerning the latter, and even though UAVs operate at lower Reynolds numbers than jet transports, adopting the BWB configuration can potentially lead to an enhanced aerodynamic efficiency compared to a typical tube-wing aircraft. Another big advantage is its greater internal volume, which allows for the installation of larger and heavier payloads.

BWBs are, by definition, tailless configurations; therefore, their design calls for a unique set of layout choices. Sweeping the wing aftwards is the most common choice, as it is even visible to the untrained eye [4,8]. In contrast to theoretical aerodynamics, where sweep is used to alleviate the compressibility effects and reduce wave drag [9], wing sweep is used in this case regardless of the operating Mach number to enhance longitudinal and lateral stability, by moving the aerodynamic to the rear and by providing a natural dihedral effect, respectively [10,11]. Moreover, by placing the control surfaces at the outboard

section of the swept wing, the layout designer can achieve adequate moment arm and, consequently, controllability.

This design choice may address many key issues of BWB design but is also linked with a critical disadvantage. That is, the wing develops a pitch-up tendency at high angles of attack that can lead to total loss of controllability and lift [10,11]. This pitch-up tendency is commonly defined as unstable pitch break and often in swept wings with high aspect ratio (AR) [12,13]. The two main mechanisms that cause this phenomenon are the spanwise flow, i.e., the flow developing from the root towards the tip of the wing, which enhances the flow separation towards the tip, and the local upwash that is produced due to the swept geometry, leading the local sections close to the wingtip to reach their maximum lift coefficients sooner and then stall. Both mechanisms cause the tip to stall first [14–16]. On the one hand, as the flow at the inboard sections remains attached, the lift production keeps increasing as the angle of attack increases. On the other hand, though, tip stalling causes the center of pressure of the wing to move forward, affecting the pitching moment of the aircraft on a progressively negative way and, ultimately, leading to unstable pitch break. The control of the aircraft is also affected in a negative way, as the control surfaces located towards the tip progressively lose their effect. The aforementioned issues pose a serious threat to BWB operation at the flight segments where the aircraft operates high angles of attack, like take-off and landing.

To counter this destructive phenomenon, several methods of active and passive flow control have been proposed. The wing fences [17,18] stop the spanwise flow development by physically obstructing its path, forcing the flow to go parallel with the fence. The vortex generators [19], the vortilons [20] and the dog-tooth configurations [21] deal with the spanwise flow by creating a vortex over the suction side of the wing, which has a similar effect with the wing fences, creating a pseudo-fence. While all the above can lead to positive results, they are means of passive flow control and, as such, affect the airflow during the whole flight. This can lead to a drag increase which can compromise the aerodynamic efficiency and the performance of the aircraft.

Another possible technique to counter the pitch break is the use of leading-edge slats [13,14,22]. Deploying slats does not only lead to the creation of vortices which work as pseudo-fences but by increasing the speed of the local airflow as well. This way, the airflow remains attached to the wing at a greater percentage of its span, tip stall is delayed and the occurrence of an unstable pitch break is either avoided or delayed. The advantage of leading-edge slats is that, as a means of active flow control technique, they can be extended on-demand during take-off and landing, to counter the risk for unstable pitch break at high angles of attack. For the remainder of the flight, they remain retracted and have little to no effect on aerodynamic performance. Their main drawback is the weight and complexity penalty that comes along with slat integration [23]; therefore, if a layout designer is to consider this technique for their trade studies, they must have a set of trends and guidelines to properly design and exploit the full potential of their advantages.

The majority of research on leading-edge slats is focused mostly on the simulation of two-dimensional multi-element airfoils [24,25], their application on wing turbines [26,27], or their effect on the noise [28]. When the use of slats on aircraft wings is investigated [22], researchers focus on lift enhancement and the pitch attitude is often neglected, as a conventional aircraft can deal with the unstable pitch break of the wing by using its tail surfaces.

In the present work, a detailed parametric investigation of leading-edge slat configurations was performed. The objectives can be briefly described as follows:

- To provide trends for the sizing of leading-edge slats on a tailless, BWB UAV configuration;
- To incorporate critical aspects of longitudinal stability in the investigation;
- To propose an efficient CFD-based methodology that can allow future researchers to replicate the analysis on different platforms during the conceptual and preliminary design phases, where both the time and the resources are usually limited.

The effect of key slat design parameters was examined using computational modeling to identify its respective effect on the angle where the pitch break appears, the speed at

which the UAV encounters pitch-break (defined as V_{stall} in the current study) and the distance between the Neutral point of each configuration and the Neutral point of the reference platform (Δx_{NP}). By using the Taguchi methodology, four design parameters were examined on three different levels. The examined parameters were the slat semi-span ($b_s/2$), the rotation of the slat element (δ_s), the extension forward of the leading edge (Δx) and the downward drop below the leading edge (Δy). Additionally, using the Pareto Analysis of Variance (ANOVA), the percentage contribution of the design parameters was defined for each of the optimized performance criteria.

2. Baseline Platform

The baseline platform utilized in this study is a fixed-wing, BWB (Blended-Wing-Body) UAV configuration. It closely resembles the RX-3 prototype, which underwent a comprehensive conceptual and preliminary design study [8]. The development process of the RX-3 was supported by applied aerodynamics investigations and parametric studies carried out at the Laboratory of Fluid Mechanics and Turbomachinery (LFMT) within the School of Mechanical Engineering at the Aristotle University of Thessaloniki (AUTH) in Greece. The design and sizing of the UAV, along with the aerodynamic, stability, and performance analyses, were conducted using established design methods and dedicated in-house tools. Moreover, the entire development process adhered to relevant airworthiness regulations. For reference, Figure 1 displays the external layout of the baseline platform, which also serves as the reference configuration in the context of the EURRICA project layout. The sweep of the wing section of the UAV was selected at 33 degrees, while the AR equaled to 8. More details about the design procedure, the tools and the layout can be found in [8]. The operating specifications of the baseline platform resembled those of tactical UAVs, as the latter are described in [29], and they are presented with detail in [8,30]. Some basic geometric, mass and performance data that are relevant to this study are presented in Table 1.

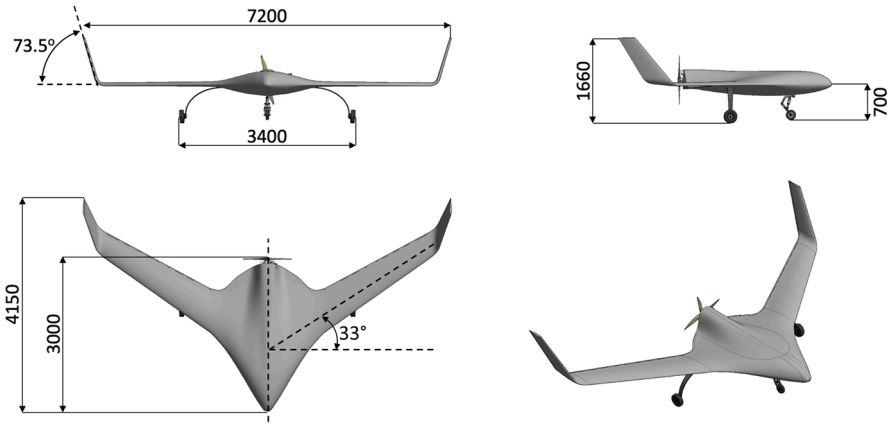

Figure 1. External layout of the tactical BWB UAV baseline platform in millimeters (mm).

Table 1. Baseline BWB UAV platform specifications.

MTOW	260	[kg]
Cruise speed	160	[km/h]
Take-off speed	108	[km/h]
Reference area (S)	4.9	[m^2]
Quarter-chord sweep angle ($\Lambda_{c/4}$)	33	[deg]
Aspect Ratio (AR)	8	[-]
Mean aerodynamic chord	1.005	[m]

3. Tools and Methods

3.1. Slat Design

According to the corresponding literature [11,16,31,32], the key slat design parameters are the slat chord (c_s), the extension forward of the leading edge (Δx or α), the downward drop below the leading edge (Δy or b), the size of the gap at the outlet of the slat (c), the rotation of the element (δ_S), the airfoil of the slats and the semi-span of the slats ($b_s/2$), as can be seen in Figure 2.

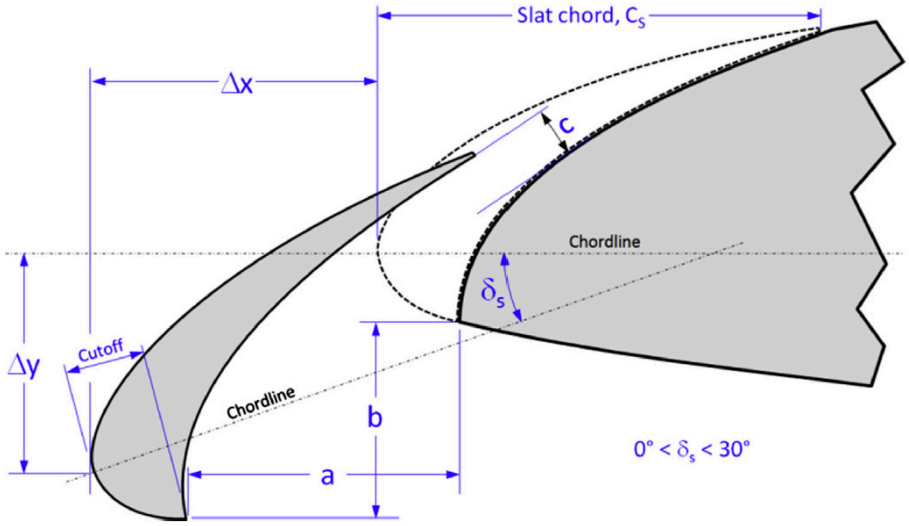

Figure 2. Slat design geometric parameters definition [11].

The size of the gap at the outlet of the slat was directly linked to the positioning of the slat element resulted from Δx, Δy and δ_S and, as such, did not serve as an independent variable in the present work. The two dimensional (2D) profile of the slat (the airfoil and the chord of the slat) was linked to the corresponding profile of the main wing. In this work, the latter derived from a given baseline platform; therefore, no further analysis was conducted on the 2D slat profile. The placement of the inboard frame of the slat on the wing was heavily affected by structural limitations, i.e., by the spanwise locations that feature a wing rib that has been properly sized to accommodate the slat structure. However, as the structural analysis of the slat is beyond the scope of this work, the root of the wing served as the inboard frame and was kept constant during the whole study.

As a result, the number of design parameters of the slat elements that were used in the current trade study was reduced from seven to four, allowing for a more focused study and leading to a major reduction in the total computational time. The orthogonal array of the Taguchi methodology was defined by the semi-span of the slats (A), the rotation of the element (B), the extension forward of the leading edge (C) and the downward drop (D).

To produce the different slat configurations for all the combinations of the selected geometric parameters, the corresponding CAD models were created using commercial 3D CAD software. The main body of the UAV was created with the use of an in-house parametric tool [8] and the slat element was then subtracted from the main wing as a distinct solid body. In the end, the slat configuration was moved and rotated appropriately to generate the desired configuration. In Figure 3, the top view of two slat configurations is indicatively presented, as a result of the CAD modeling. Configuration 2 is presented on the right with blue, while configuration 6 is on the left with red.

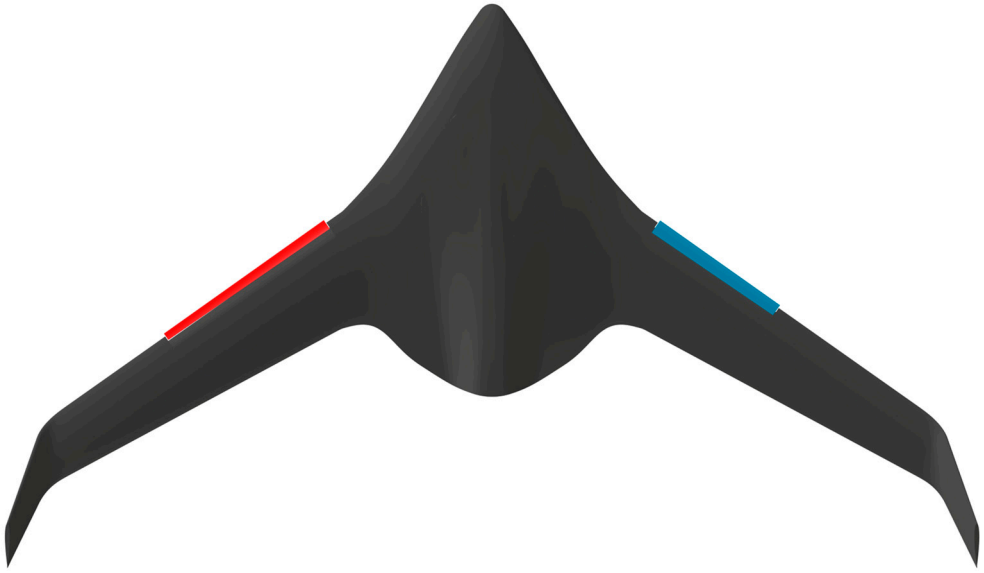

Figure 3. Indicative comparison between two different configurations of the L_9 array.

3.2. Taguchi Methodology

In contemporary aircraft design, the widespread utilization of advanced computational methods and experiments is prevalent. These techniques enable crucial optimization and trade studies to take place, but they come with limitations due to their considerable demands on computational time, resources and human effort. Consequently, the design space is often constrained, as highlighted in the examination of winglet sizing studies that are presented in [30]. The complexity and the cost of the trade studies is further increased when rapid, lower-fidelity methods (e.g., vortex lattice methods) cannot be trusted to model complex 3D configurations, as is the case of the slats and their effect on the pitch break.

When the whole design space is under investigation, for a full factorial generic optimization problem, the number N of the possible combinations that occur for L number of levels of the design parameters and m number of design parameters is equal to the expression shown in Equation (1).

$$N = L^m \tag{1}$$

To avoid the expenses associated with a full factorial analysis and simultaneously explore the entire design space, Taguchi introduced a standardized Design of Experiments (DOE) method [33]. This widely adopted approach in the industry facilitates the development of high-quality products by maximizing their robustness and making them less susceptible to uncontrollable factors, all at a relatively lower cost. Taguchi's method achieves this by employing a special set of Orthogonal Arrays (OAs) that define the minimum required "experiments" for the chosen design parameters (Table 2). These experiments ensure that the conclusions drawn from the reduced "experimental" space remain valid across the entire design space. ensuring that the conclusions derived from the reduced "experimental" space are valid over the entire design space. It is important to clarify that the use of the Taguchi method itself is not a novel concept, as it is a well-established DOE method extensively employed in various industries. However, the proposed overall approach, which combines Taguchi with ANOVA to determine the percentage contribution of the leading-edge slats design parameters to stability and low-speed performance, is truly unique and original. This specific combination has not been previously discussed in published aeronautical literature.

Table 2. Indicative comparison between a full factorial and a Taguchi experimental design.

Factors	Levels	Full Factorial Design	Taguchi Design
2	2	4 (2^2)	4
3	2	8 (2^3)	4
4	2	16 (2^4)	8
7	2	128 (2^7)	8
15	2	32.768 (2^{15})	16
4	3	81 (3^4)	9

The initial step in creating an orthogonal array involves determining the total degrees of freedom, which establishes the minimum number of required "experiments" to investigate the chosen design parameters. For each design parameter (A, B, C, etc.), the degrees of freedom are calculated as the number of levels minus one (Equation (2)), where *i* stands for the respective parameter (A, B, C, etc.). Therefore, the overall degrees of freedom are obtained by summing up the degrees of freedom of the main effects of the design parameters, along with an additional degree of freedom associated with the overall mean [34].

$$df_i = number\ of\ levels\ of\ parameter\ i - 1 \quad (2)$$

The second step involves determining the suitable layout for the Orthogonal Array (OA), which is determined by the total degrees of freedom and the number of design parameters. The number of rows in the OA must be at least equal to the total degrees of freedom, while the number of columns is based on the factors and their levels. The design engineers select the specific design parameters, considering relevant aspects in the field, theory, and common practice [10,35]. Concerning the current study, the design parameters defined in the previous section are presented in Table 3. The values of each design parameter level are selected based on reference platform and manufacturability restrictions and general guides for slats design [11,16,31,32]. In conclusion, the combination of the design parameters and their levels (four parameters with three levels each) led to an L_9 orthogonal array for the current trade studies (Table 4). Thus, nine different slats configurations were examined and their effect on the aerodynamic performance of the examined platform was extracted. It is essential to note that by employing the Taguchi method, the total number of cases to be examined was significantly reduced from 81 to just 9, in contrast to the full factorial approach. This substantial reduction in cases drastically decreased the effort required for CAD and CFD analysis.

Table 3. Design parameters and their levels under investigation.

Parameters	Levels		
	1	**2**	**3**
A, Slat Semispan [% b/2]	45	60	75
B, δ_s [degrees]	10	20	30
C, Δx [% $\bar{c}$]	1	3	5
D, Δy [% $\bar{c}$]	0	2	4

Table 4. L_9 Orthogonal Array.

Configuration	A	B	C	D
1	45	10	2	0
2	45	20	4	2
3	45	30	6	4
4	60	10	4	4
5	60	20	6	0

Table 4. *Cont.*

Configuration	A	B	C	D
6	60	30	2	2
7	75	10	6	2
8	75	20	2	4
9	75	30	4	0

3.3. CFD Methodology

The aerodynamic behavior of each configuration was investigated using high-fidelity, CFD computations. In the present study, the steady-state Reynolds Averaged Navier–Stokes (RANS) equations were solved, with the adoption of an appropriate turbulence model, necessary for their closure. The model of Spalart and Allmaras (SA) [36] was selected, the one-equation eddy viscosity model. One transport equation (Equation (3)) was used for the calculation of the viscosity variable $\widetilde{\nu}$. The use of the model is widely spread for external aerodynamics flows and has been experimentally validated in low freestream Reynolds number applications.

$$\frac{\partial}{\partial t}\left(\rho\widetilde{\nu}\right) + \frac{\partial}{\partial x_i}\left(\rho\widetilde{\nu}u_i\right) = G_\nu + \frac{1}{\sigma_{\widetilde{\nu}}}\left[\frac{\partial}{\partial x_j}\left\{\left(\mu + \rho\widetilde{\nu}\right)\frac{\partial\widetilde{\nu}}{\partial x_j}\right\} + C_{b2}\rho\left(\frac{\partial\widetilde{\nu}}{\partial x_j}\right)^2\right] - Y_\nu + S_{\widetilde{\nu}} \quad (3)$$

The CAD models were imported in BETA ANSA pre-processing software (v19.1.0, Root, Switzerland) to properly discretize the surrounding control volume and generate the corresponding computational mesh (Figure 4). As the UAV was symmetrical, only half of the model was employed in the simulations, resulting in approximately 28 million computational cells for all tested cases. This study employed a combination of structured and unstructured meshing techniques. An unstructured mesh philosophy was used to discretize the majority of the computational domain, as it provided greater flexibility for discretizing the flow domain around the complex 3D configurations, such as the region between the slat element and the main body (Figure 4b). On the contrary, a structured mesh was applied in close proximity to the UAV surface. This may locally cause an increase in the number of elements, but was used to better capture the flow and its sharp changes (steep gradients) inside the boundary layer (Figure 5b). More specifically, concerning the boundary layer discretization, the y+ parameter did not exceed a value of 5 at any point of the model surface and, in general, was kept below 1. The reason for this was to ensure that the viscous sublayer region was adequately modeled [37]. Apart from thickness, the size of surface elements ranged from 1 mm at areas such as the trailing edge, to 30 mm at regions like the middle part of the main body. Concerning the leading edge curvature resolution, it was discretized into a minimum of 25 elements to ensure accurate modeling, both at the slat and the wing leading edge. The mesh size was based on the grid dependency study presented in [30] for the baseline configuration. The results are indicatively shown in Figure 6 for the Lift and Drag coefficients, with the red marker dictating the selected grid for this study.

The solution was performed with the Ansys CFX software (Release 18.2, Academic Multiphysics Campus Solution, Canonsburg, PA, USA), using a coupled pressure-based solver, and second-order spatial discretization schemes for the continuity, x-, y- and z-momentum and viscosity variable transport equations. The examined configurations were modeled in a wide range of angles of attack, which spanned between −4 degrees and 16 degrees, so that the pitch break occurred. The atmospheric conditions and the flight speed that were used for this investigation corresponded to take-off and landing segments of a typical flight, where the use of slats was expected, i.e., sea level conditions. It must be noted at this point that, for research purposes, a follow-up analysis could also be conducted at different flight altitudes to compare flight performance. However, the

baseline configuration of this study was not expected to deploy slats at another flight phase and, consequently, this follow-up analysis was not carried out in this paper.

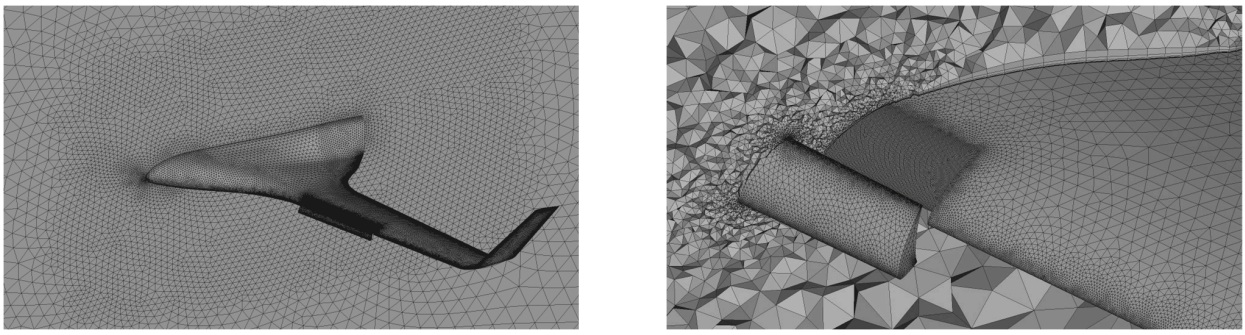

(**a**) (**b**)

Figure 4. Computational mesh (**a**) around the UAV and (**b**) slat detailed view.

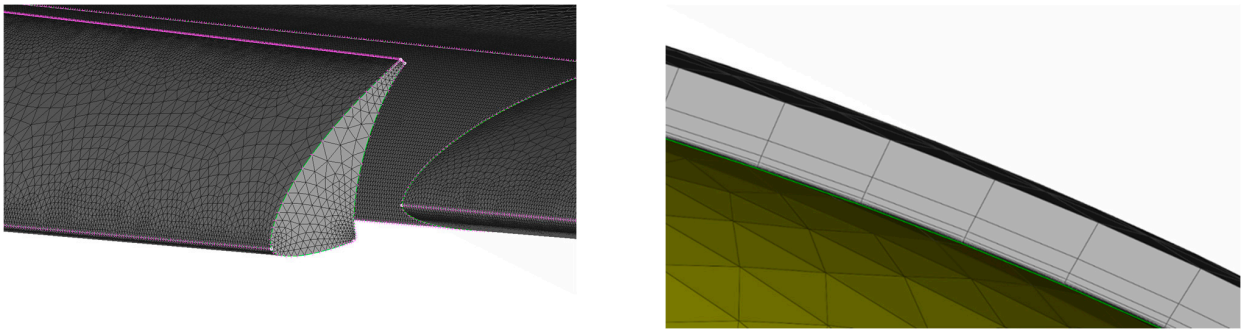

(**a**) (**b**)

Figure 5. Detailed view of the mesh (**a**) over the slat element and (**b**) the boundary layer.

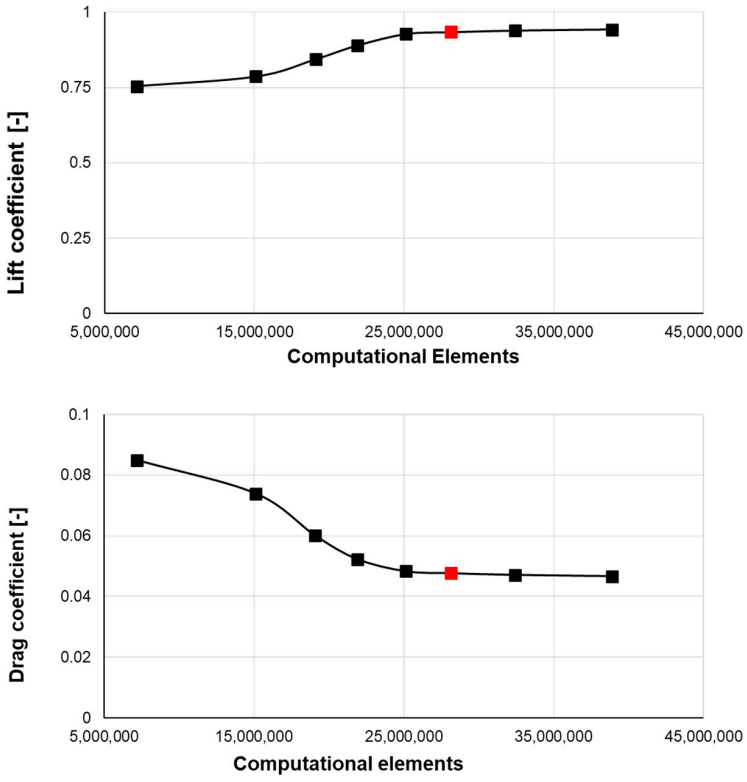

Figure 6. Results of the grid-dependency study for the Lift (**top**) and Drag (**bottom**) coefficients.

The boundary and initial conditions are summed up in Table 5, also including the turbulence boundary conditions at the inlet [38]. It is important to address the computational modeling's fidelity at this stage. While utilizing a more sophisticated approach, such as employing the Unsteady RANS and advanced turbulence models or a Reynolds Stress Model (RSM), could potentially produce more accurate results in predicting the impact of slats on aerodynamics and stability, the authors of the current work chose not to focus on providing such detailed outcomes. As stated in the introduction, the primary goal was to conduct a comparative research study that strikes a balance between adequate fidelity (using a well-established turbulence model for aeronautical applications) and computational efficiency. This approach allows the identification of key trends and ensures the overall method's reproducibility during the conceptual and preliminary design phases of UAV configurations, where time and resources are limited.

Table 5. Boundary conditions for CFD modeling.

Parameter	Take-Off Set	Units
Freestream velocity	100 27.778	[km/h] [m/s]
Altitude	0	[m]
Ambient pressure	101.3	[kPa]
Ambient temperature	15	[°C]
Eddy Viscosity Ratio	0.21	[-]
Fractional Intensity	0.01	[-]

3.4. SNR and ANOVA

The Signal-to-Noise Ratio (SNR) was suggested by Taguchi for the analysis of the results. The SNR generally represents the efficiency factor and a quality measure connected with the loss function. By maximizing the SNR, the losses related to the procedure were minimized. The "experimental" observations were converted to SNR, following three basic, different definitions depending on the desirable direction of the results (Equations (4)–(6)). The logarithmic transformation of the observations in SNR strengthens the prediction of the performance criteria improvement.

$$\text{Smaller the better}: \; SNR = -10\log_{10}\sum_1^n y^2 \tag{4}$$

$$\text{Nominal the better}: \; SNR = -10\log_{10}\sum_1^n \frac{\overline{Y}}{s_y^2} \tag{5}$$

$$\text{Bigger the better}: \; SNR = -10\log_{10}\sum_1^n \frac{1}{y^2} \tag{6}$$

In this specific case, the term y refers to the estimated performance criteria for each configuration and n to the number of configurations under investigation. Furthermore, $\overline{Y}$ is the mean value and S_Y^2 is the variance of each performance criterion (Equations (7) and (8)) [39].

$$\overline{Y} = \frac{\sum_1^k y}{k} \tag{7}$$

$$S_Y^2 = \frac{\sum_1^k \left(y - \overline{Y}\right)^2}{k} \tag{8}$$

Concerning the performance criteria of the current study, for the optimization of the pitch-break angle, the 'Bigger the better' definition was used, whereas for the optimization of the V_{stall} and the Δx_{NP}, the 'Smaller the better' definition was applied. For each performance criterion, the combination of the design parameters with the highest SNR was the optimum one and corresponded to the best performance with the minimum variation.

Additionally, the study included an ANOVA [34,40] to analyze the findings and draw conclusions concerning the optimal combination for each performance criterion. ANOVA is a statistical technique primarily employed for analyzing "experimental" data and examining the influence of design parameters on the overall variation of the results. In this research, a simplified version of ANOVA known as Pareto ANOVA [40] was utilized. Based on the Pareto principle, this method provides a quick and straightforward way to analyze the results of parametric trade studies. Importantly, the Pareto ANOVA does not require an F-test, allowing for the determination of the statistical significance of each design parameter for every performance criterion.

In the current study, an ANOVA was conducted for the angle where the pitch break appeared, the speed at which the UAV had pitch-break (which is named as V_{stall} in the current study) and the distance between the Neutral point of each configuration and the Neutral point of the reference platform (Δx_{NP}), taking into concern the SNR analysis results, yielding the importance and the percentage contribution of slat semispan ($b_S/2$, Δs, Δx and Δy).

Following the methodology presented in [40], let i stand for the number of parameters and j stand for the number of levels of each design parameter so that i and j range from 1 to 4 and 1 to 3, respectively. Hence, following the well-established ANOVA methodology, the contribution of each design parameter is calculated using Equation (9).

$$Percentage\ contribution = \frac{SS_i}{SS} \cdot 100 \tag{9}$$

The terms SS_i and SS represent the sum of squares of each design parameter and the total sum of squares, respectively, due to variation about the overall mean. The exact values of SS_i and SS are calculated using Equations (10) and (11).

$$SS_i = \sum_1^3 \left(SNR_{ij} - \overline{SNR}\right)^2 \tag{10}$$

$$SS = \sum_1^{27} \left(SNR_i - \overline{SNR}\right)^2 \tag{11}$$

Finally, SNR_{ij} is the average SNR of the ith parameter at the jth level, and the overall mean SNR is calculated using Equation (12).

$$\overline{SNR} = \frac{\sum_1^{27} SNR_i}{27} \tag{12}$$

The above procedure is conducted for each one of the performance criteria, yielding two percentage contributions in the current study.

4. Results

The basic aerodynamic coefficients, such as the lift and drag forces and the pitching moment, were extracted from the CFD simulations for the total of the configurations of the nine configurations. The lift and the drag coefficients were calculated using the reference area shown in Table 1. Moreover, Table 1 also presents the mean aerodynamic chord that was used for the calculation of the pitching moment coefficient. The lift coefficient, the drag polars of these configurations and the trim diagrams are presented in Figures 7–9, compared with the baseline geometry without slats. The center of gravity at take-off was used for this analysis, which was located at 1790 mm from the UAV apex. As the UAV was designed to be inherently stable during the whole duration of a typical flight, the same conclusions can be extracted for the landing configuration as well.

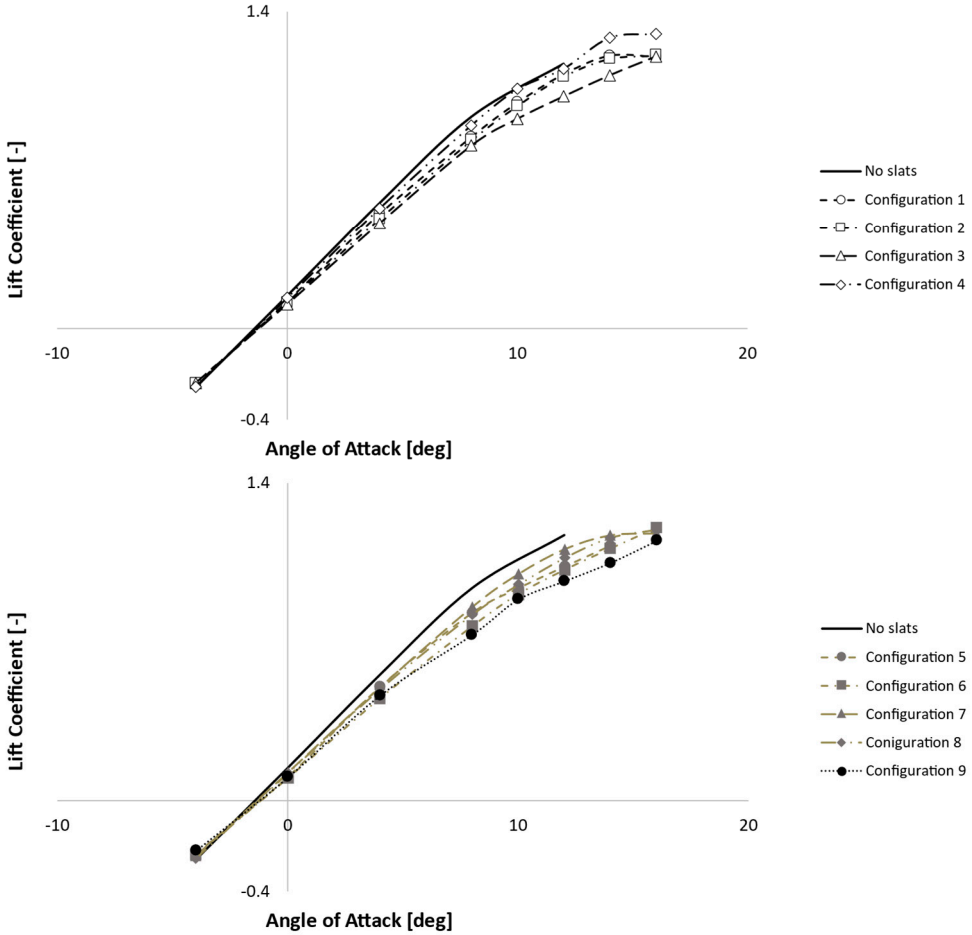

Figure 7. Lift coefficient as a function of angle of attack for configurations 1–4 compared with baseline (**top**) and configurations 5–9 compared with baseline (**bottom**).

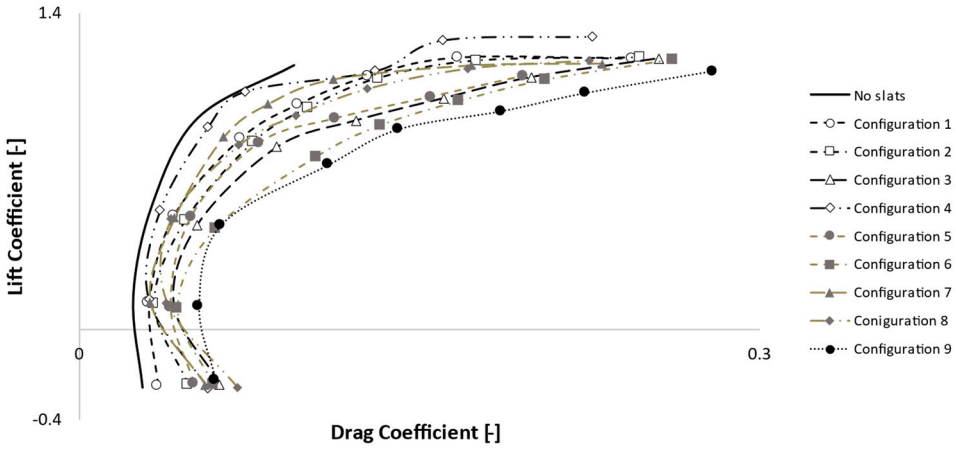

Figure 8. Drag polars of the examined configurations.

The use of slats led to a slight reduction in the slope of the lift coefficient in the linear region of the curve. This slope reduction became more evident as the rotation of the slat element increased, reaching as much as 16% for configuration 9. This can be attributed to the fact that, at small angles of attack, the slat suction side was placed almost perpendicularly to the airflow and did not contribute to lift production. As the angle of attack increased, the gap of the slat became more effective, as the UAV did not reach its aerodynamic stall.

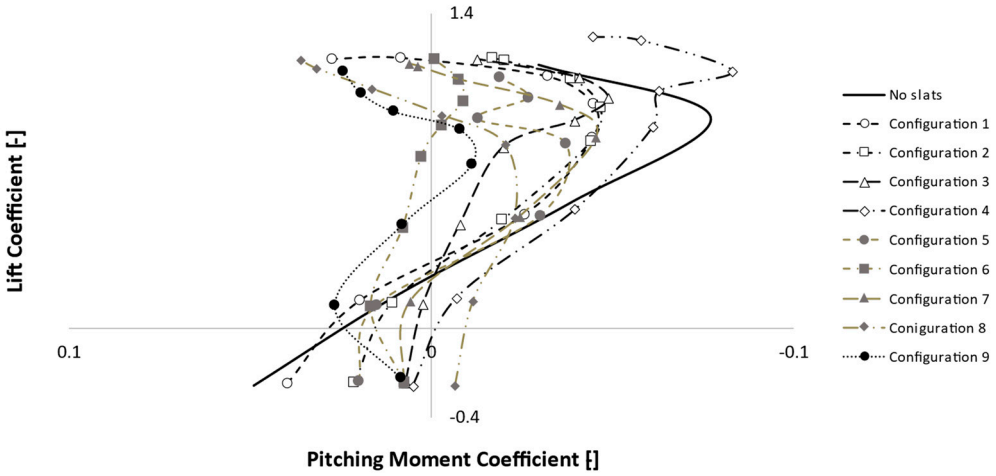

Figure 9. Lift Coefficient vs. Pitching Moment Coefficient for all of the examined configurations.

The effect of the slats on the lift coefficient became evident at angles of attack higher than 8 degrees. As can be seen in Figure 7, for all the of the examined configurations, the maximum lift coefficient either remained the same or was slightly increased, as was the case with configuration 4. However, it would be wrong to consider these angles of attack as operational because, as will be discussed in the next paragraph, pitch break already occurred. The total drag of the UAV increased because of the slats extension (Figure 8), but the authors did not consider this to be a major issue for the performance of the vehicle, as the devices are expected to be used during take-off and landing flight segments.

Figure 9 primarily shows that, as expected, the use of slats had a major impact on the angle of attack where pitch break occurred. The pitch break remained unstable, the stall progression of some configurations was more gradual and "soft" [9], depending on the corresponding design parameters. For example, the pitch break on configuration 2 (Figure 10, top) was delayed for about 2 degrees and seemed to be smoother than the baseline geometry, as the pitching moment caused smaller deviations to appear in this range. In contrast, configuration 8 (Figure 10, bottom) was expected to have pitch break between 4 and 8 degrees of angle of attack, while the Neutral point of the UAV moved forwards, leading closer to neutral static stability. An important note at this point is the fact that even though all configurations affected the static stability of the UAV, the use of slats did not lead to instability at any point.

The SNR analysis was conducted to define the optimum combination of the design parameters for each performance criterion (Pitch break angle, V_{stall} and Δx_{NP}). From the SNR analysis, the SNR of each configuration for each performance criterion was calculated (Table 6). It was found that the mean SNR for Pitch break angle was 18.99 Db, for the V_{stall}, it was −30.02 dB and for Δx_{NP}, it was 26.21 dB.

Table 6. Performance criteria and calculated SNR.

Configuration	Pitch Break Angle	SNR	V_{stall}	SNR	Δx_{NP}	SNR
	[°]	[dB]	[m/s]	[dB]	[m]	[dB]
1	10	20.00	29.73	−29.46	0.02	34.42
2	10	20.00	29.94	−29.53	0.03	29.90
3	12	21.58	29.33	−29.35	0.08	22.27
4	12	21.58	27.73	−28.86	0.04	28.40
5	8	18.06	32.66	−30.28	0.03	29.12
6	12	21.58	29.48	−29.39	0.09	21.11
7	8	18.06	32.17	−30.15	0.04	28.40
8	8	18.06	32.84	−30.33	0.10	20.35
9	4	12.04	43.67	−32.80	0.08	21.94

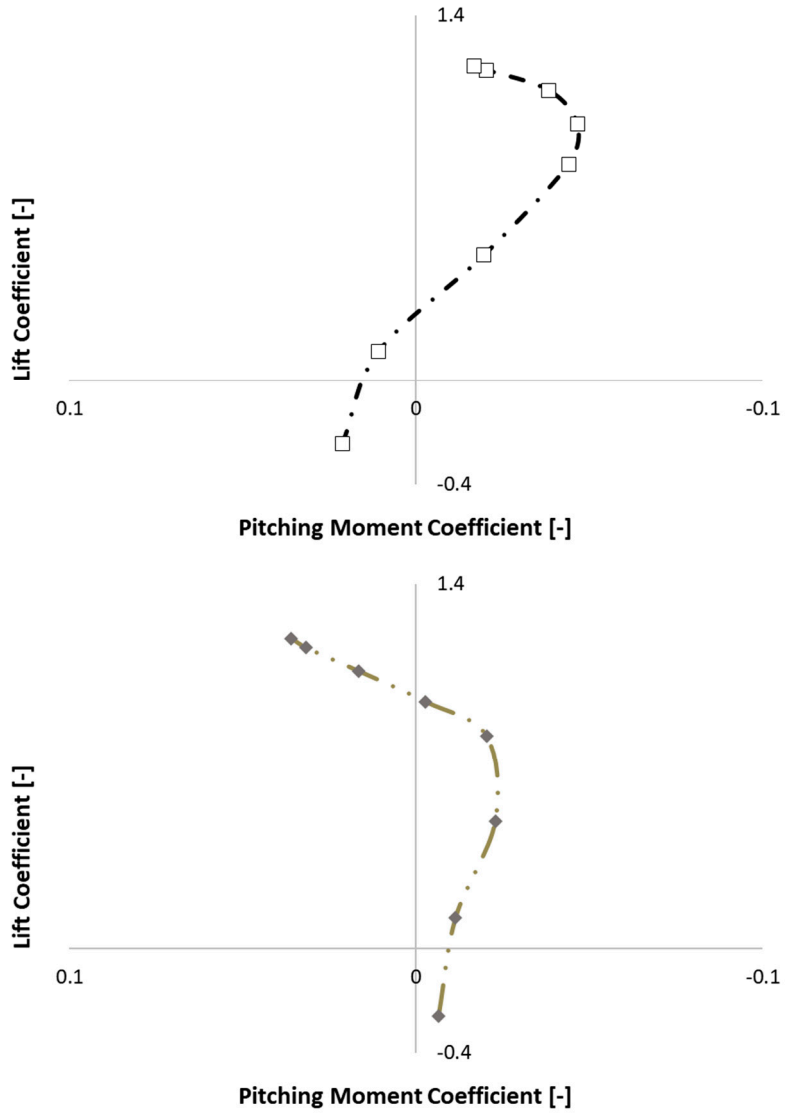

Figure 10. Lift Coefficient vs. Pitching Moment Coefficient for configurations 2 (**top**) and 8 (**bottom**).

For the optimization of the pitch-break angle, the 'Bigger the better' definition of SNR was used, while for the optimization of the V_{stall} and the Δx_{NP}, the 'Smaller the better' definition was selected. The results of the SNR analysis for each parameter individually are presented in Tables 7–9. Delta was equal to the difference between the maximum and the minimum SNR value of each parameter. The rank of each design parameter revealed which one affected the response characteristic more and it was defined by the fraction of each parameter Delta divided by the sums of all the parameters' Deltas.

Table 7. Response table for pitch break angle.

Level	A ($b_S/2$)	B (δ_S)	C (Δx)	D (Δy)
1	20.53	19.88	19.88	16.70
2	20.41	18.71	17.87	19.88
3	16.05	18.40	19.24	20.41
$Delta_{max}$	4.47	1.48	2.01	3.71
Rank	1	4	3	2
Contribution ratio [%]	38.34	12.68	17.20	31.79

Table 8. Response table for V_{stall}.

Level	A ($b_S/2$)	B (δ_S)	C (Δx)	D (Δy)
1	−29.45	−29.49	−29.73	−30.85
2	−29.51	−30.04	−30.40	−29.69
3	−31.09	−30.51	−29.93	−29.51
$Delta_{max}$	1.65	1.02	0.67	1.34
Rank	1	3	4	2
Contribution ratio [%]	35.24	21.87	14.29	28.61

Table 9. Response table for Δx_{NP}.

Level	A ($b_S/2$)	B (δ_S)	C (Δx)	D (Δy)
1	−29.45	−29.49	−29.73	−30.85
2	−29.51	−30.04	−30.40	−29.69
3	−31.09	−30.51	−29.93	−29.51
$Delta_{max}$	1.65	1.02	0.67	1.34
Rank	1	3	4	2
Contribution ratio [%]	35.24	21.87	14.29	28.61

The effect of the design parameters on the performance criteria is shown in plot form in Figures 11–13. The optimum level of each parameter for each response characteristic was the one with the maximum SNR. The pitch break angle and the V_{stall} had similar behavior as they both took their maximum value at the first level for A ($b_S/2$), B (δ_S) and C (Δx), and at the third level for D (Δy). Δx_{NP} performance metric took its maximum value at the first level for A ($b_S/2$), B (δ_S) and D (Δy), and at the second level for C (Δx).

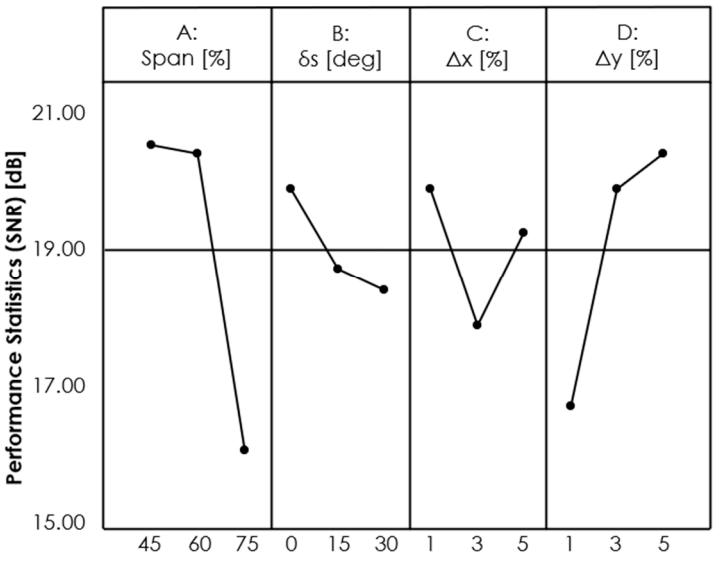

Figure 11. Effect of the design parameters on the pitch break angle.

The optimum design parameter levels combinations for each examined performance criterion are summed up in Table 10. The combination $A_1B_1C_1D_3$ optimized the pitch break angle, according to the "Bigger is Better" condition and the corresponding SNR analysis. In a similar way, the same combination ($A_1B_1C_1D_3$) was the optimum for the V_{stall} metric, while the $A_1B_1C_2D_1$ was the optimum combination for Δx_{NP}, by the "Smaller is Better" definition of the SNR. The smaller semi-span and rotation of the slat elements seemed to be the preferable choice, while the translation of the slat element forward from

the leading-edge can be kept at the smaller percentages for the optimization of the stability at this range of angles of attack.

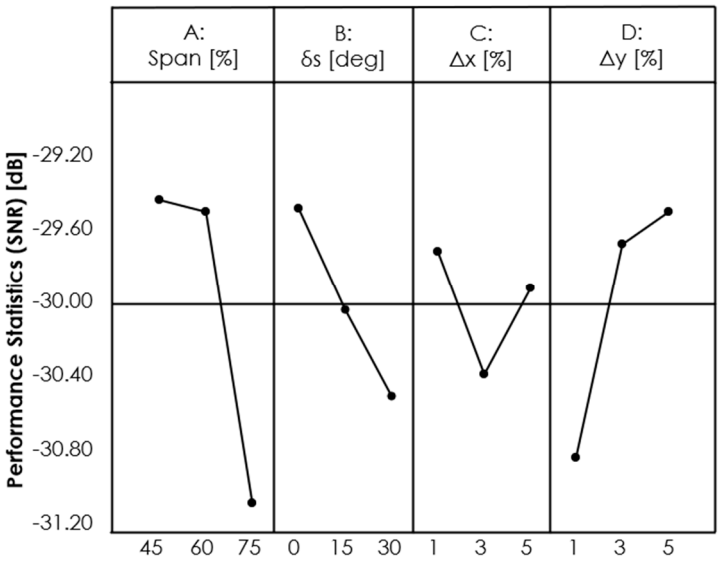

Figure 12. Effect of the design parameters on V_{stall}.

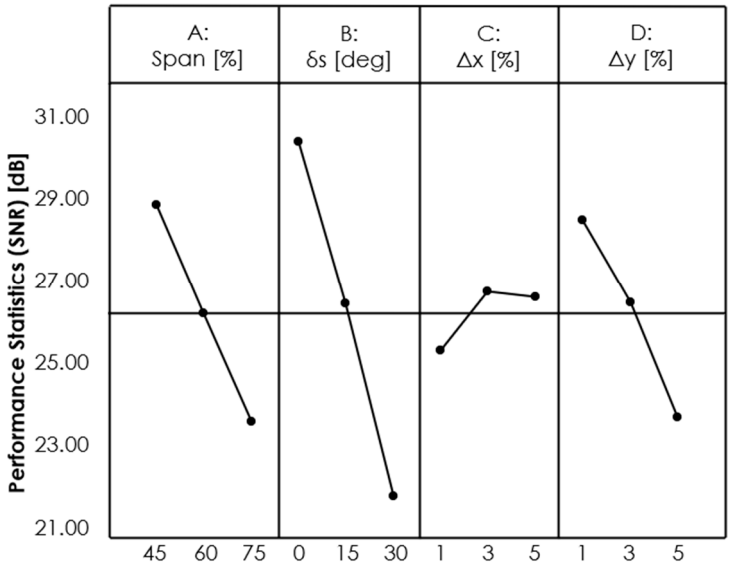

Figure 13. Effect of the design parameters on Δx_{NP}.

Table 10. Optimum design parameter combinations for the optimization of the performance criteria.

	Design Parameters			
	A (Span)	**B (δs)**	**C (Δx)**	**D (Δy)**
Pitch break angle				
Optimum level	1	1	1	3
Optimum value	45	0	1	5
Contribution [%]	38.34	12.68	17.20	31.79
V_{stall}				
Optimum level	1	1	1	3
Optimum value	45	0	1	5

Table 10. *Cont.*

	Design Parameters			
	A (Span)	**B (δs)**	**C (Δx)**	**D (Δy)**
Contribution [%]	35.24	21.87	14.29	28.61
Δx_{NP}				
Optimum level	1	1	2	1
Optimum value	45	0	3	1
Contribution [%]	26.22	42.76	7.18	23.84

The Pareto ANOVA results are presented in Figure 14, where the effect of design parameters on each performance criterion is specifically shown. According to the ANOVA, the pitch-break angle was mostly affected by the semi-span of the slat element (A) and the Δy (D), while the other two parameters had a similar, smaller contribution. Similarly, the semi-span (A) was the main factor that affected the V_{stall} metric, with the second most effective parameter being the Δy (D). For this metric, the rotation of the slat (B) contributed more than the Δx (C). The Δ_{XNP} was affected mostly by the δ_s (B), while the semi-span (A) and the Δy (D) contributed approximately the same at this metric. Finally, the Δx (C) seemed to have the smallest effect compared to the other parameters.

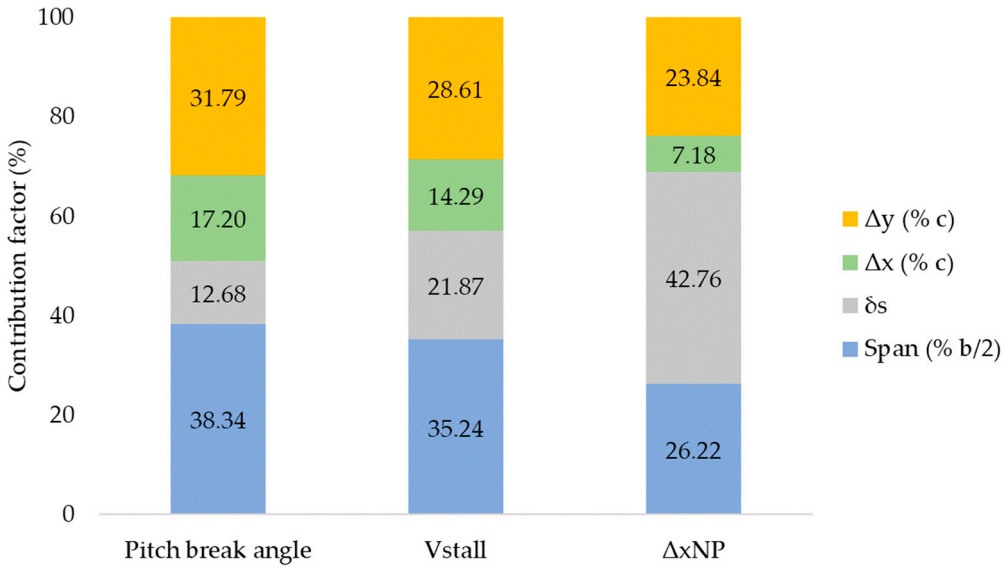

Figure 14. Contribution of the design parameters on the performance criteria.

5. Conclusions

This study presented a parametric, CFD-aided investigation of leading-edge slats conducted on a BWB UAV baseline platform. The slats were used primarily to enhance the longitudinal stability of the UAV at high angles of attack and expand its operating range. Using the Taguchi method, four different design parameters were examined and their effect on pitch break, static stability and overall performance of the UAV at high angles of attack was investigated. The various configurations were analyzed using computational modeling and the corresponding aerodynamic and stability coefficients were calculated. The combinations that maximized the pitch break angle and minimized V_{stall} and Δx_{NP}, respectively, were defined as a result of SNR analysis. Finally, a Pareto ANOVA was implemented to calculate the percentage contributions of the design parameters on each performance criterion. The main conclusions of this study are listed as follows:

- The use of an optimized slat configuration can be used to considerably expand the operating range of a tailless UAV configuration. Using non-optimized slat design values, however, can lead in a reduction in aerodynamic performance.

- The use of slats affects the slope of the pitching moment curve, but it does not result in an unfavorable behavior (static instability).
- The optimum combination of design parameters for the maximization of pitch break angle is $A_1B_1C_1D_3$ and the optimum level values are $b_s/2 = 45\%$, $\delta_s = 0^\circ$, $\Delta x = 1\%$ and $\Delta y = 5\%$.
- The optimum combination of design parameters for the minimization of V_{stall} is $A_1B_1C_1D_3$ and the optimum level values are $b_s/2 = 45\%$, $\delta_s = 0^\circ$, $\Delta x = 1\%$ and $\Delta y = 5\%$.
- The optimum combination of design parameters for the minimization of Δx_{NP} is $A_1B_1C_2D_1$ and the optimum level values are $b_s/2 = 45\%$, $\delta_s = 0^\circ$, $\Delta x = 3\%$ and $\Delta y = 1\%$.
- The parameter that affects the pitch break angle and the V_{stall} the most is the $b_s/2$ with a contribution factor of 38.34% and 35.24%, respectively.
- The parameter that affects the Δx_{NP} the most is the δ_s with a contribution factor of 42.76%.
- The use of high-fidelity CFD simulations for the trade studies of the geometry of the leading-edge slats combined with the DOE resulted in a considerably lower amount of computational time. The design space is limited from eighty-one to just nine configurations by the implementation of the Taguchi methodology, resulting in an 89% reduction in the total computational effort.

The next steps of the current research will be focused on the addition of more geometric parameters in the parametric investigation, like the airfoil of the slat element. The use of a full-span slat will also be considered. The authors would also like to investigate the optimal slat design for each flight segment, like take-off, climb, approach and landing. This could also involve investigations at different flight altitudes to compare the slat performance. Finally, the structural implementations of the use of leading-edge slats can also be investigated, with emphasis on the actuation and the weight penalty for each of the alternative designs.

Author Contributions: Conceptualization, S.A. and S.K.; methodology, P.P. and S.K.; software, S.A.; validation, S.K., P.P. and K.Y.; investigation, S.A.; resources, S.A.; data curation, S.A. and S.K.; writing—original draft preparation, S.A. and S.K.; writing—review and editing, P.P. and K.Y.; visualization, S.A. and S.K.; supervision, P.P.; project administration, P.P.; funding acquisition, P.P. and K.Y. All authors have read and agreed to the published version of the manuscript.

Funding: The work presented in this paper was funded by the Hellenic Foundation for Research and Innovation (HFRI), partially in the framework of the EURRICA research project under the "2nd Call for H.F.R.I. Research Projects to support Post-Doctoral Researchers" (Project Number: 00745) and partially in the framework of the 3rd Call for HFRI PhD Fellowships (Fellowship Number: 6179).

Data Availability Statement: Data available on request due to restrictions related to the details of the baseline platform. The data presented in this study are available on request from the corresponding author.

Conflicts of Interest: The authors declare no conflict of interest.

References

1. Liebeck, R.H. Design of the Blended Wing Body Subsonic Transport. *J. Aircr.* **2004**, *41*, 10–25. [CrossRef]
2. Qin, N.; Le Moinge, A. Spanwise Lift Distribution for Blended Wing Body Aircraft. *J. Aircr.* **2005**, *42*, 356–365. [CrossRef]
3. Reist, T.A.; Zingg, D.W. Aerodynamic design of blended wing body and lifting-fuselage aircraft. In Proceedings of the 34th AIAA—Applied Aerodynamics Conference, Session: Innovative Aerodynamic Concepts Designs, Washington, DC, USA, 13–17 June 2016. AIAA 2016-3874.
4. Faggiano, F.; Vos, R.; Baan, M.; van Dijk, R. Aerodynamic Design of a Flying V Aircraft. In Proceedings of the 17th AIAA Aviation Technology, Integration, and Operations Conference, Denver, CO, USA, 5–9 June 2017; American Institute of Aeronautics and Astronautics Inc. (AIAA): Reston, VA, USA, 2017. AIAA 2017-3589. [CrossRef]
5. Wakayama, S. Blended-wing-body optimization problem setup. In Proceedings of the 8th Symposium on Multidisciplinary Analysis and Optimization, Long Beach, CA, USA, 6–8 September 2000; p. 4740.

6. Suewatanakul, S.; Porcarelli, A.; Olsson, A.; Grimler, H.; Chiche, A.; Mariani, R.; Lindbergh, G. Conceptual Design of a Hybrid Hydrogen Fuel Cell/BatteryBlended-Wing-Body Unmanned Aerial Vehicle—An Overview. *Aerospace* **2022**, *9*, 275. [CrossRef]
7. Cummings, R.; Liersch, C.; Schütte, A. Multi-Disciplinary Design and Performance Assessment of Effective, Agile NATO Air Vehicles. *Aerosp. Sci. Technol.* **2020**, *99*, 105764. [CrossRef]
8. Panagiotou, P.; Mitridis, D.; Dimopoulos, T.; Kapsalis, S.; Dimitriou, S.; Yakinthos, K. Aerodynamic design of a tactical Blended-Wing-Body UAV for the aerial delivery of cargo and lifesaving supplies. In Proceedings of the AIAA Scitech 2020 Forum, Orlando, FL, USA, 6–10 January 2020.
9. Anderson, J.D. *Fundamentals of Aerodynamics*, 6th ed.; WCB/McGraw-Hill: Boston, MA, USA, 2011; ISBN 9780073398105.
10. Raymer, D. *Aircraft Design: A Conceptual Approach, Sixth Edition*; American Institute of Aeronautics and Astronautics: Reston, VA, USA, 2018.
11. Gudmundsson, S. *General Aviation Aircraft Design*, 2nd ed.; Butterworth-Heinemann: Oxford, UK, 2022.
12. Shortal, J.A.; Maggin, B. *Effect of Sweepback and Aspect Ratio on Longitudinal Stability Characteristics of Wings at Low Speeds*; Defense Technical Information Center: Fort Belvoir, VA, USA, 1946; NACA TN-1093.
13. Furlong, G.C.; Mchugh, J.G. *A Summary and Analysis of the Low-Speed Longitudinal Characteristics of Swept Wings at High Reynolds Number*; Defense Technical Information Center: Fort Belvoir, VA, USA, 1957; NACA TR-1339.
14. Koven, W.; Graham, R.R. *Wind-Tunnel Investigation of High-Lift and Stall-Control Devices on a 37 Degree Sweptback Wing of Aspect Ratio 6 at High Reynolds Numbers*; Defense Technical Information Center: Fort Belvoir, VA, USA, 1948; NACA RM-L8D29.
15. Haines, A.B. *Some Notes on the Flow Patterns Observed over Various Swept-Back Wings at Low Mach Numbers (in the R.A.E. 10ftx7ft High Speed Tunnel*; Cranfield University: Cranfield, UK, 1954; R&M No. 3192.
16. Hoerner, S.F.; Borst, H.V. *Fluid Dynamic Lift*; Hoerner, L.A., Ed.; Hoerner Fluid Dynamics: Bricktown, NJ, USA, 1985.
17. Dickson, J.K.; Sutton, F.B. *The Effect of Wing Fences on the Longitudinal Characteristics at Mach Numbers Up to 0.92 of a Wing-Fuselage-Tail Combination Having a 400 Sweptback Wing with Naca 64a Thickness Distribution*; National Advisory Committee for Aeronautics: Washington, DC, USA, 1955.
18. Walker, M.; Bons, J. The Effect of Passive and Active Boundary-Layer Fences on Swept-Wing Performance at Low Reynolds Number. In Proceedings of the AIAA Scitech 2018 Forum, Kissimmee, FL, USA, 8–12 January 2018.
19. Goharshadi, M.; Mirzaei, M. Delaying the Stall of a Low-Wing Aircraft Using A Novel Powerful Vortex Generator. *Inventions* **2022**, *7*, 95. [CrossRef]
20. Phillips, E.; Wygnanski, I.J.; Menge, P.M.; Taubert, L. Passive and Active Leading Edge devices on a simple swept back wing. In *AIAA Aviation 2019 Forum*; American Institute of Aeronautics and Astronautics: Reston, VA, USA, 2019; p. 3393, NACA-RM-L52C25.
21. Jaquet, B.M. *Effects of Chord Discontinuities and Chordwise Fences on Low-speed Static Longitudinal Stability of an Airplane Model Having a 35 Degree Sweptback Wing*; Defense Technical Information Center: Fort Belvoir, VA, USA, 1952; NACA-RM-L52C25.
22. Alam, M.; Kara, K.; Alexander, A. Reduction of spanwise flow over a swept wing using an air curtain produced by rectangular slot. In *AIAA AVIATION 2022 Forum*; American Institute of Aeronautics and Astronautics: Reston, VA, USA, 2022; p. 3296.
23. Rudolph, P.K. *High-Lift Systems on Commercial Subsonic Airliners*; NASA: Washington, DC, USA, 1996; NASA-CR-4746.
24. Malik, M.; Lin, R. Transition prediction on the slat of a high-lift system. *J. Aircr.* **2004**, *41*, 1384–1392. [CrossRef]
25. Renukumar, B.; Bramkamp, F.; Hesse, M.; Ballmann, J. Effect of flap and slat riggings on 2-D high-lift aerodynamics. *J. Aircr.* **2006**, *43*, 1259–1271.
26. Steiner, J.; Viré, A.; Benetti, F.; Timmer, N.; Dwight, R. Parametric slat design study for thick-base airfoils at high Reynolds numbers. *Wind Energ. Sci.* **2020**, *5*, 1075–1095. [CrossRef]
27. Wang, H.; Jiang, X.; Chao, Y.; Li, Q.; Li, M.; Zheng, W.; Chen, T. Effects of leading edge slat on flow separation and aerodynamic performance of wind turbine. *Energy* **2019**, *182*, 988–998. [CrossRef]
28. Li, W.; Guo, Y.; Liu, W. On the mechanism of acoustic resonances from a leading-edge slat. *Aerosp. Sci. Technol.* **2021**, *113*, 106711. [CrossRef]
29. Verstraete, D.; Palmer, J.L.; Hornung, M. Preliminary Sizing Correlations for Fixed-Wing Unmanned Aerial Vehicle Characteristics. *J. Aircr.* **2018**, *55*, 715–726. [CrossRef]
30. Panagiotou, P.; Antoniou, S.; Yakinthos, K. Cant angle morphing winglets investigation for the enhancement of the aerodynamic, stability and performance characteristics of a tactical Blended-Wing-Body UAV. *Aerosp. Sci. Technol.* **2022**, *123*, 107467. [CrossRef]
31. Olson, L.E.; McGowan, P.R.; Guest, C.J. *Leading-Edge Slat Optimization for Maximum Airfoil Lift*; NASA: Washington, DC, USA, 1979; No. A-7753.
32. Weick, F.E.; Sanders, R. *Wind-Tunnel Tests on Combinations of a Wing with Fixed Auxiliary Aerofoils Having Various Chords and Profiles*; NASA: Washington, DC, USA, 1934; NACA-TR-472.
33. Roy, R.K. *Primer on the Taguchi Method*, 2nd ed.; Society of Manufacturing Engineers: Deadborn, MI, USA, 2010; ISBN 9780872638648.
34. Phadke, M.S. *Quality Engineering Using Robus*, 1st ed.; Prentice Hall: Englewood Cliffs, NJ, USA, 1989; ISBN 0-13-745167-9.
35. Austin, R. *Unmanned Aircraft Systems, UAVS Design, Development and Deployment*; Wiley: Chichester, UK, 2010.
36. Spalart, P.R.; Allmaras, S.R.; Reno, J. One-Equatlon Turbulence Model for Aerodynamic Flows. In Proceedings of the 30th Aerospace Sciences Meeting Exhibit, Reno, NV, USA, 6–9 January 1992; p. 23.
37. Wilcox, D.C. *Turbulence Modeling for CFD*, 2nd ed.; DCW Industries: La Canada, CA, USA, 1998.

38. Rumsey, C.L.; Spalart, P.R. Effective inflow conditions for turbulence models in aerodynamic calculations. *AIAA J.* **2009**, *45*, 2544–2553.
39. Nelson, R.C. *Flight Stability and Automatic Control*; McGraw-Hill: New York, NY, USA, 1997; ISBN 0070462739.
40. Vankanti, V.K.; Ganta, V. Optimization of Process Parameters in Drilling of GFRP Composite Using Taguchi Method. *J. Mater. Res. Technol.* **2014**, *3*, 35–41. [CrossRef]